Available online at www.sciencedirect.com
SCIENCE DIRECT®
Journal of Magnetic Resonance 159 (2002) 36–45
JMR Journal of Magnetic Resonance
www.academicpress.com

Spectrally resolved velocity exchange spectroscopy of two-phase flow

A.A. Khrapitchev,[a,*] S. Han,[b] S. Stapf,[b] and B. Blümich[b]

[a] School of Chemical and Physical Sciences, Victoria University, P.O. Box 600, Wellington, New Zealand
[b] Rheinisch-Westfälische Technische Hochschule Aachen, Lehrstuhl für Makromolekulare Chemie, ITMC, Worringerweg 1, D-52074 Aachen, Germany

Received 17 March 2002; revised 5 August 2002

Abstract

The Velocity EXchange SpectroscopY (VEXSY) technique, which provides a means to correlate macroscopic molecular displacements measured during two intervals separated by a variable mixing period, has been applied for the first time to a system of two-phase flow. The chemical shift difference between water and methyl protons has been exploited to simultaneously determine the probability of displacements, or propagator, of both components in a water/silicone oil mixture flowing through a glass bead pack. The joint two-time probability densities as well as the conditional probabilities of velocities show a clearly distinct dispersion behaviour of both fluids which is a consequence of the different wetting properties of the fluids with respect to the glass surface of the bead pack.

Keywords: Two-phase flow; VEXSY; Propagator; Chemical resolution; q space imaging

1. Introduction

Pulsed field gradient (PFG) NMR has been applied for more than a decade as a versatile method for investigating not only averaged quantities of random molecular diffusion processes, but also to unravel more complicated patterns in directed laminar or turbulent flow, often in the presence of structured and porous media. Based on statistical descriptions of fluid transport and dispersion processes by means of distributions of displacements, or *propagators* [1], the influence of the surrounding medium on the behaviour of a flowing fluid has been studied, and combinations of imaging and velocity encoding have been suggested, being motivated to a large degree by petrophysical [2–4] or engineering problems [5,6]. More recently, the potential of multiple encoding of displacements has been exploited to correlate different quantities to each other—positions [7], displacements in different directions [8,9] and at different times [10]. It is particularly this latter method, Velocity EXchange SpectroscopY or VEXSY, and its one dimensional [11–13], two-dimensional [14,15] and multi-dimensional [16,17] modifications which has been found useful for detailed investigations of dispersion processes in porous media not being accessible by conventional techniques. However, one of the main advantages of NMR, namely its ability to provide chemically selective information from an analysis of the spectral fingerprint, has until now not been exploited in combination with such multiple-encoding, correlating techniques, despite the fact that most of the described PFG methods are based on pure phase-encoding of displacements and retain the full frequency information.

In this paper, we demonstrate the—to our knowledge—first application of the VEXSY sequence to the simultaneous measurement of dispersion of a two-phase fluid system within a porous medium, using a mixture of water and silicone oil flowing through a random packing of monodisperse glass beads. We show that it is possible to clearly distinguish between the temporal correlation of velocities in the wetting and the non-wetting phase, and to attribute particular features of the joint two-time probability density and the conditional probability to different subsets of fluid elements of both phases.

* Corresponding author.
E-mail addresses: alex.khrapitchev@vuw.ac.nz (A.A. Khrapitchev), songi@dirac.cchem.berkeley.edu (S. Han), sstapf@mc.rwth-aachen.de (S. Stapf), bluemich@mc.rwth-aachen.de (B. Blümich).

1090-7807/02/$ - see front matter
PII: S1090-7807(02)00002-2

2. Theory

The basic principle of the measurement of displacements by means of pulsed magnetic field gradient (PFG) NMR can be understood as an (at least) twofold encoding of position at different times allowing the system to evolve in between these time points. If such an encoding is brought about by two narrow gradient pulses with wave vectors of opposite sign, $k_1 = -k_2$, separated by an interval Δ, the accumulated phase shift of each spin isochromat will vanish for static spins but a remaining phase shift will be observable which is proportional to the displacement of spins during Δ, $\boldsymbol{R} = r_2 - r_1$. If the wave vector given by the PFG pair $\boldsymbol{q}$ is defined as [18] $\boldsymbol{q} = (k_2 - k_1)/2$, where $\boldsymbol{q} = (1/2\pi)\gamma \boldsymbol{g}\delta$ with $\boldsymbol{g}$ and δ denoting the strength and the duration of each PFG, respectively, and γ the gyromagnetic ratio, the normalized signal intensity $E(\boldsymbol{q})$ can be written as

$$E(\boldsymbol{q}) = S(\boldsymbol{q})/S(0) = \int \overline{P_1}(\boldsymbol{R}, \Delta) \exp[\mathrm{i}2\pi \boldsymbol{q}\boldsymbol{R}]\, \mathrm{d}\boldsymbol{R}, \tag{1}$$

where the propagator $\overline{P_1}(\boldsymbol{R}, \Delta)$ is defined as [1]

$$\overline{P_1}(\boldsymbol{R}, \Delta) = \int \rho(r_1) P(r_1|r_2, \Delta)\, \mathrm{d}r_1. \tag{2}$$

$\rho(r_1)$ is the probability density for starting positions, while $P(r_1|r_2, \Delta)$ is the conditional probability for positional change from r_1 to r_2 during Δ. The propagator is obtained from the signal intensity by Fourier transformation with respect to $\boldsymbol{q}$, with the usual assumption $\delta \ll \Delta$. One possible realization of this encoding scheme is given by the stimulated-echo sequence shown in Fig. 2a.

In order to compare two displacements, or velocities, with each other, this basic module can be repeated within one pulse sequence, now encoding displacements in two intervals Δ separated by a mixing time, τ_m. This method has been dubbed VEXSY, [10] and its stimulated-echo version [19] is shown in Fig. 2b. If both gradient pairs are varied independently of each other, defining wave vectors $\boldsymbol{q}_1$ and $\boldsymbol{q}_2$, respectively, the signal is given by

$$E(\boldsymbol{q}_1, \boldsymbol{q}_2) = \int\int \overline{P_2}(\boldsymbol{R}_1, \Delta; \boldsymbol{R}_2, \Delta; \tau_\mathrm{m}) \exp[\mathrm{i}2\pi \boldsymbol{q}_1 \boldsymbol{R}_1] \times \exp[\mathrm{i}2\pi \boldsymbol{q}_2 \boldsymbol{R}_2]\, \mathrm{d}\boldsymbol{R}_1 \mathrm{d}\boldsymbol{R}_2. \tag{3}$$

The two-time joint probability density of finding displacements $\boldsymbol{R}_1$ in the first *and* $\boldsymbol{R}_2$ in the second interval of duration Δ, $\overline{P_2}(\boldsymbol{R}_1, \Delta; \boldsymbol{R}_2, \Delta; \tau_\mathrm{m})$, can be rewritten as

$$\overline{P_2}(\boldsymbol{R}_1, \Delta; \boldsymbol{R}_2, \Delta; \tau_\mathrm{m}) = \overline{P_1}(\boldsymbol{R}_1, \Delta) \mathscr{P}_V(\boldsymbol{R}_1, \Delta | \boldsymbol{R}_2, \Delta; \tau_\mathrm{m}). \tag{4}$$

Clearly, the conditional probability $\mathscr{P}_V(\boldsymbol{R}_1, \Delta \mid \boldsymbol{R}_2, \Delta; \tau_\mathrm{m})$ of a fluid element having $\boldsymbol{R}_2$ in the second interval *given that* it has had $\boldsymbol{R}_1$ in the first interval, is simply obtained from dividing $\overline{P_2}(\boldsymbol{R}_1, \Delta; \boldsymbol{R}_2, \Delta; \tau_\mathrm{m})$, by the one-dimensional propagator, $\overline{P_1}(\boldsymbol{R}_1, \Delta)$. In the discussion of our experimental results, we will present both functions for the sake of a more clearer description of the details of the dispersion process. For a more elaborate discussion of the VEXSY and related schemes, we refer the reader to [20].

It might be noted at this stage that the pulse sequences shown in Fig. 2 contain phase encoding steps exclusively, so that the chemical shift information is retained in the echo signal acquired at the end of the sequence. The VEXSY scheme is thus generally speaking a three-dimensional experiment, with two dimensions in $\boldsymbol{q}$ space and one time dimension. The mixing time τ_m represents, in principle, a fourth variable, but is only used as a parameter in our experiments which were performed at certain, selected values of τ_m.

3. Experimental

A glass tube of 12 mm inner diameter and 250 mm length with two symmetrically positioned inlets on one side was filled with glass beads of $(400 \pm 50)\,\mu$m diameter. The sample was confined between glass frits acting as a diffusor in order to provide an even distribution of streamlines at the inlet and to avoid hold-up of particles at the outflow (see Fig. 1). The porosity of the packing was determined by weighting the sample before and after the addition of water and was found to be 45%. The sample was prepared by adding a mixture of water and beads to the water-filled container and the packing was regularly stirred to avoid trapping of air bubbles. After fixing the frits, the two inlets of the glass container were connected to one pump each (BVP-Z and Reglo-Z, Ismatec) by silicone rubber tubes of approximately 2 m length, providing a constant volume flow rate of both fluids through the bead pack sample. The pumps were connected to reservoirs of bidistilled water and silicone oil Baysilone M10 produced by Bayer with a viscosity of $\eta = 10$ mPa s. All experiments were performed with total volume flow rates between about 1.0 and 1.5 l/h. First, the flow behaviour of water as the only phase has been investigated. Next, water flow has been stopped and

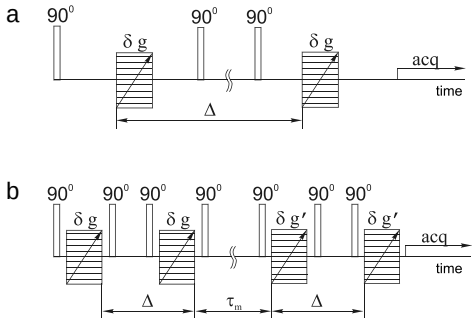

Fig. 1. Schematic sketch of the sample used for single- and two-phase flow experiments.

been replaced by oil flow of the same volume flow rate. The measurements were performed several hours after no removal of water from the sample cell could be detected. This corresponded to a residual water volume concentration of $S_{wi} = (8 \pm 1)\%$. Oil has then been replaced by water as the flowing phase, the residual oil volume concentration measured under these conditions has been $S_{or} = (19 \pm 2)\%$. In the final step, simultaneous flow of water and oil at flow fractions of 0.43 and 0.57, respectively, was maintained and the experiments were started after several hours of equilibration. The volume concentrations inside the bead pack were found to be $S_w = (52 \pm 3)\%$ and $S_o = (48 \pm 3)\%$, respectively. Due to the immiscibility of the two fluids, alternating water and oil bubbles formed at the inlet of the sample. However, the combined effect of the glass frits and the dispersion of the fluid mixture in the bead pack itself led to a sufficient mixing so that no indication of large scale (>2 mm) heterogeneities in the fluid distribution of the moving phase were found at the observation slice (15 mm width) situated 12 cm downstream from the inlet. This was checked by acquiring a series of spectroscopically resolved Hahn echoes which showed no detectable variation of the fluid volumes ratio on time scales between seconds and minutes.

The NMR experiments were performed on a DMX 300 MHz Bruker spectrometer equipped with a horizontal super wide bore 7 T magnet. A commercial microimaging gradient system was used, providing a maximum gradient strength of 1.2 T/m. In order to minimize the influence of transverse relaxation in the presence of the background field gradients generated by the glass/liquid interface, stimulated-echo versions of all pulse sequences had been used throughout. One-dimensional PGSTE experiments were performed with the pulse sequence shown in Fig. 2a, the duration of the gradient pulses, δ, being set to 0.25 ms. For the two-dimensional VEXSY experiments, the sequence shown in Fig. 2b has been employed with an encoding time of

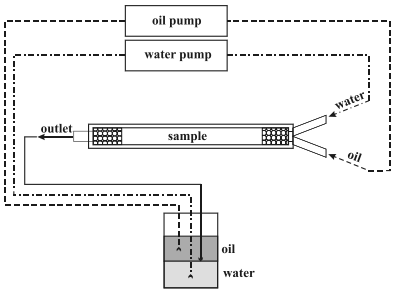

Fig. 2. (a) Schematic RF and gradient pulses sequence for a simple PGSTE NMR experiment in which the gradient pulse area (δg) is stepped and z storage is used for the encoding period. (b) Schematic RF and gradient pulses sequence for a general double PGSE NMR experiment in which the gradient pulse areas (δg) and ($\delta g'$) are stepped independently of each other; z storage is used for the both encoding and mixing periods.

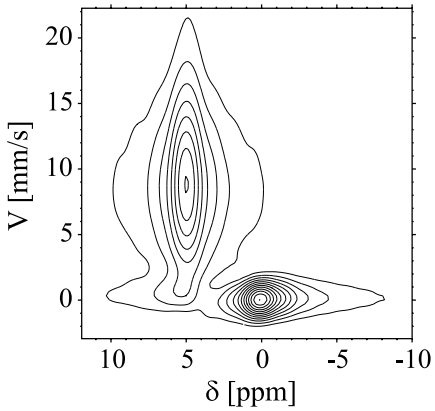

Fig. 3. Two-dimensional representation of a spectrally resolved propagator; the chemical shift is shown on the abscissa axis, the displacement on the ordinate axis. The peak on the left-hand represents flowing water, the peak on the right-hand side arises from the static residual oil phase.

$\Delta = 16$ ms. This time was long enough to allow the determination of the full displacement propagator, yet corresponded to an average displacement during the encoding time of about 150 μm which is still small compared to the bead size. One can thus assume that velocity changes of the fluid elements during Δ are minor (see the discussion in the following section). Pulsed field gradients were applied parallel to the average pressure gradient throughout, hereby measuring displacements Z parallel to the main flow axis. In Fig. 3 we show a typical representation of the one-dimensional propagator measurement with the chemical shift drawn along the horizontal axis: the peak on the right-hand side corresponds to residual oil, while water is seen to flow with an highest-probability velocity of 9 mm/s. In some regions of the spectrum, the lines do overlap. A line fitting routine has therefore been applied which allowed to determine the relative contributions of the two spectral lines which then led to a correct representation of the propagators.

4. Results and discussion

4.1. One-dimensional propagators of single- and two-phase flow

Following the order of measurements outlined in Section 3, we will first compare the situation of one-phase flow in the presence of two-phase saturation. For silicone oil as the flowing phase, we observed a residual volume concentration of water of $S_{wi} = (8 \pm 1)\%$. The propagator $\overline{P}_1(Z, \Delta)$ of the water distribution necessarily has to be centered about zero displacements as no net flow occurs. The upper part of Fig. 4 indeed, indicates such a behaviour, the propagator can be approximated by a Gaussian curve and is found to be symmetric with the exception of

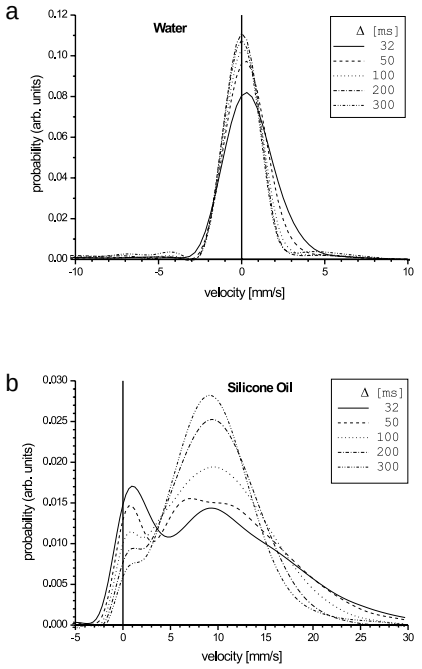

Fig. 4. One-dimensional propagators $\overline{P_1}(Z,\Delta)$ for flow of silicone oil in packed beads of 400 μm diameter in the presence of irreducible water at $S_{wi} = (8 \pm 2)\%$. The average velocity and Péclet number are $\overline{v^*} = 9.5$ mm/s and Pe = 15000 for the oil phase. The propagators were obtained with encoding times Δ varied as indicated employing the double-PGSE pulse sequence shown in Fig. 2a.

the shortest encoding time, where an asymmetry toward positive displacements is seen. This is probably explained as an artifact coming from the silicone oil spectral line which is dominating and most difficult to separate from the water contribution particularly under these conditions. The magnitude of the velocities, ranging up to approximately 2 mm/s, exceeds the one expected from pure random self-diffusion with a diffusion coefficient of $D_0 = 2.1 \times 10^{-9}\,\mathrm{m^2/s}$ by about one order of magnitude: for unhindered self-diffusion, $\langle Z^2 \rangle = 2D_0\Delta$ so that one expects a velocity scale of $\sqrt{\langle Z^2 \rangle}/\Delta = \sqrt{2D_0/\Delta}$ or between 0.12 and 0.36 mm/s for the Δ values used in this study. One therefore has to assume that momentum transport takes place at the oil/water interfaces due to the friction between both fluids, and that the flowing oil phase drives circulating motions of the water pools if they can indeed be regarded as droplets resting at particular positions in the bead packing.

The velocity distribution function of silicone oil is shown in the bottom half of Fig. 4. For all encoding times, it retains an average velocity of $\overline{v^*} = (9.5 \pm 0.5)$ mm/s as determined from the first moment of the propagators, in equivalence to the results derived from the volume flow rate. The shape of the propagator is best described by a bimodal behaviour with one peak at small (in fact, nearly zero) velocity and a second peak centered about the average velocity. The peak corresponding to the quasi-static fluid elements decreases in intensity as the encoding time increases, but is still visible at $\Delta = 300$ ms. This evolution is a familiar observation and has been reported repeatedly in the literature [21–23]. It can be explained by the presence of liquid pools essentially not taking part in the main flow process, being only loosely connected to the backbone of streamlines. The time necessary for the "slow" molecules to mix into the flowing part of the fluid is determined by the size of the pools and the self-diffusion coefficient of the fluid. D_0 of silicone oil has been measured as $2 \times 10^{-10}\,\mathrm{m^2/s}$, corresponding to displacements on the order of 10 μm for the longest Δ.

If the distribution of phases is reversed, i.e. with water being the flowing and silicone the non-flowing phase, the propagators change to the shape presented in Fig. 5. The net displacement for silicone oil is now zero, as expected, while the width of the velocity distribution is almost identical to the one of water in Fig. 4, despite the smaller self-diffusion coefficient of oil. This again supports the view of a circulating motion of the non-moving phase driven by the moving phase. Such a circulating motion has, for instance, been observed for water drops falling in air [24] where the vortex patterns could indeed be visualized directly, while it was found to be absent for the non-moving fluid of two-phase flow in rocks where the droplet size is much smaller [25,26]. We merely mention this observation here because it is beyond the scope of this work, and refer to a more thorough investigation in a forthcoming paper.

The propagator of the flowing water phase shown in the upper part of Fig. 5 resembles that for flowing oil in

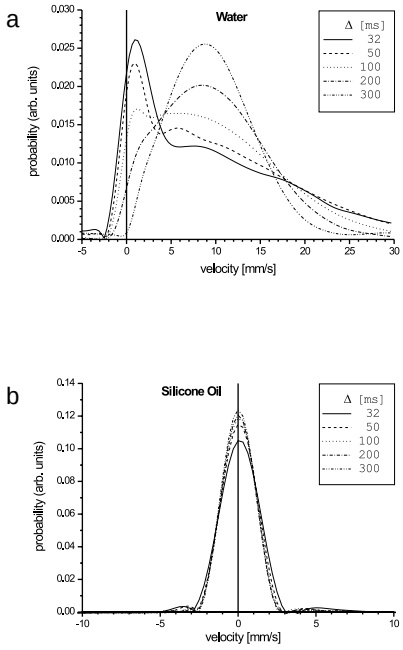

Fig. 5. As in Fig. 4, but for water flowing in the presence of residual oil at $S_{or} = (19 \pm 2)\%$. The average velocity and Péclet number are $\overline{v^*} = 11.0$ mm/s and Pe = 1400 for the water phase.

Fig. 4 at first sight, but gradual differences can be observed. The intensity of the quasi-static peak is higher at short encoding times but then decreases faster with growing Δ. One reason for this is the above mentioned fact that the time necessary for leaving the quasi-static fluid pools depends on the self-diffusion coefficient; which is ten times larger for water. Furthermore, for untreated silica glass the silicone oil represents the wetting phase, i.e. it will preferentially be found near the surface of the glass beads. Due to the non-slip condition of Newtonian fluids at the glass interface, this fraction of the oil phase will possess small velocities and contribute to the quasi-static peak.

The pore space available for the flowing water phase (Fig. 5), on the other hand, is different from the one for the flowing oil phase (Fig. 4). In the case of full oil-wetting, water does not reach the bead surface and is forced to flow within the pore space of an array of beads "enlarged" by the oil surface layer. If oil is flowing, the residual water is expected to be distributed in droplets not connected to the bead surface, adding further obstacles to the oil flow.

One further difference between the two cases is the somewhat smaller effective porosity for the flowing water phase, because of the residual oil fraction of $S_{or} = (19 \pm 2)\%$ being larger than the residual water fraction in the opposite case. At identical flow rates, one therefore expects an average velocity which is between 10 and 15% higher than for the flowing oil phase. The average velocity of $\overline{v^*} = (11.0 \pm 0.5)$ mm/s determined from the propagator experiments coincides well with this estimation and agrees with the value computed from the volume flow rate.

The observed effects are corroborated by a comparison with single-phase flow of water through a packing of the same glass beads under almost identical conditions. As is discussed in more detail in [8,27] and [28], the shape of the propagator and its evolution with increasing encoding time is mainly given by the dimensionless Péclet number which is defined by

$$\mathrm{Pe} = \frac{\overline{v^*} L}{D_0}, \tag{5}$$

where L is the characteristic size of the system, conventionally defined as $L = \phi d/(1-\phi)$ with the bead diameter d and the porosity ϕ. Taking the reduced porosity of $0.45 \times 0.81 = 0.36$ into account, one finds $\mathrm{Pe} \approx 1400$. This is compared to single-phase flow of water with a very similar flow rate of the same Péclet number so that a direct comparison is possible. The velocity distribution functions for this single-phase flow in the absence of oil is shown in Fig. 6a for comparison. One observes an almost exponential shape of the propagator for short encoding times and a slightly slower decay of the quasi-static peak with growing Δ. The latter might be a consequence of the different morphology of

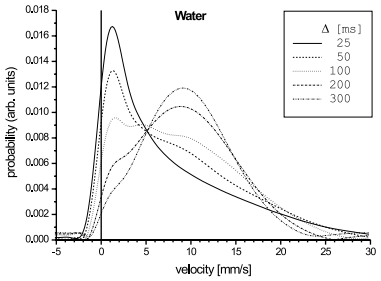

Fig. 6. As in Fig. 4, but for single-phase flow of water. The average velocity and Péclet number are $\overline{v^*} = 9$ mm/s and $\mathrm{Pe} = 1400$.

the pore space: if the wetting oil phase fills up the smallest gaps between the glass beads, these are not accessible to water anymore so that the trapping effect on water is smaller in the two-phase situation. The deviation from the exponential shape of the single-phase flow reported in the literature [21–23], can either also be due to a faster mixing between the quasi-static and the moving fluid fractions, or is a feature immanent to the true velocity distribution of the water phase itself.

The shapes of the propagators of water and oil change significantly if both liquids are flowing simultaneously with relative volume flow rates of 0.43 and 0.57; the results are presented in Fig. 7. From integrating the signal intensity in the absence of velocity encoding, one obtains volume fractions of $S_w = (52 \pm 3)\%$ and $S_o = (48 \pm 3)\%$; the volumetrically determined average velocities are (9 ± 1) mm/s for water and (13 ± 1) mm/s for silicone oil. The quasi-static component is found to be much more persistent for the oil phase and in fact hardly decreases in intensity even for $\Delta = 300$ ms, leaving a long tail which

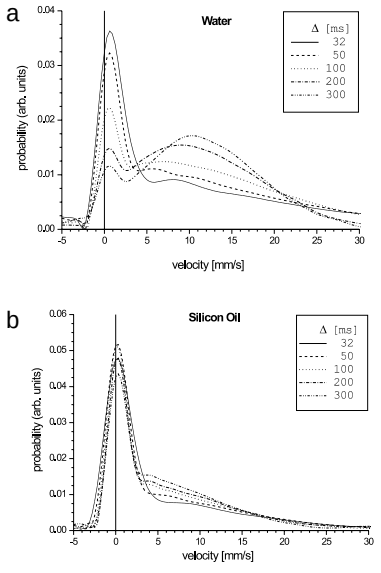

Fig. 7. As in Fig. 4, but for two-phase flow of water and oil leading, to volume fractions of $S_w = (52 \pm 3)\%$ and $S_o = (48 \pm 3)\%$. The average velocities and Péclet numbers are $\overline{v^*} = (9 \pm 1)$ mm/s and $\mathrm{Pe} \approx 550$ for the water phase, and $\overline{v^*}(13 \pm 1)$ mm/s and $\mathrm{Pe} \approx 7000$ for the oil phase.

stems from fluid elements possessing large velocities. Due to outflow effects, the relative intensity of the fastest fluid elements is possibly underestimated so that the average velocity determined from the propagator shape is somewhat smaller than the expected value. For the water phase, the build-up of the high-velocity Gaussian component is much faster; still, the fraction of slow molecules is more prominent than in the case of non-flowing oil (Fig. 5). Assuming that both fluids flow in continuous phases, it can be understood how the reduced available space for each fluid delays the mixing process for molecules between streamlines and a full sampling of the whole velocity distribution. However, more detailed conclusions can not be drawn from the one-dimensional data alone.

4.2. VEXSY of single- and two-phase flow

We now turn to discussing the results of experiments performed under identical conditions, but employing the two-dimensional VEXSY technique. The shape of the two-time joint probability density, $\overline{P_2}(Z_1, \Delta; Z_2, \Delta; \tau_m)$, is shown along with the conditional probability function, $\mathscr{P}_V(Z_1, \Delta | Z_2, \Delta; \tau_m)$, for silicone oil flowing in the presence of residual water in Fig. 8. Velocities in the first interval Δ are plotted along the abscissa axis, those in the second interval along the ordinate axis. The velocity distribution of water is centered around zero, as expected, with no clear indications of correlations between initial and final velocities discernible. These would show up in a functional relation of the conditional probability such as a positive or negative slope of the contour lines. Horizontal contour lines, on the other hand, indicate the absence of correlation between velocities. Within the central part of the displacement spectrum, contour lines are indeed horizontal. Outer contour lines representing larger velocities are influenced by the dominating oil peak, in particular for the plots of $\mathscr{P}_V(Z_1, \Delta | Z_2, \Delta; \tau_m)$, which involve a division by the one-dimensional propagator. Therefore, they will not be taken into consideration here.

The distribution functions for the flowing oil phase are plotted in the second and fourth column of Fig. 8. For the shortest mixing time, the two-time probability density $\overline{P_2}(Z_1, \Delta; Z_2, \Delta; \tau_m)$ is aligned along the main diagonal which represents fluid elements having not changed their velocity. The broadening is due to dispersion already taking place during the encoding intervals Δ themselves. With increasing τ_m, a triangular pattern develops. The loss of correlations can be more clearly seen in the plot of $\mathscr{P}_V(Z_1, \Delta | Z_2, \Delta; \tau_m)$, where an evolution of the alignment of the contour lines from the main diagonal toward the horizontal axis is found. This process can best be discussed by considering the characteristic time for the dispersion process which is given by the time it takes a molecule moving with $\overline{v^*}$ to travel a distance equivalent to the bead diameter,

$$\tau_c = d/\overline{v^*}, \tag{6}$$

which is about 42 ms. This timescale has been found to be a good approximation for the decay of the velocity autocorrelation function [29], while a distribution of correlation times $P(\tau_c)$ is more appropriate to describe a

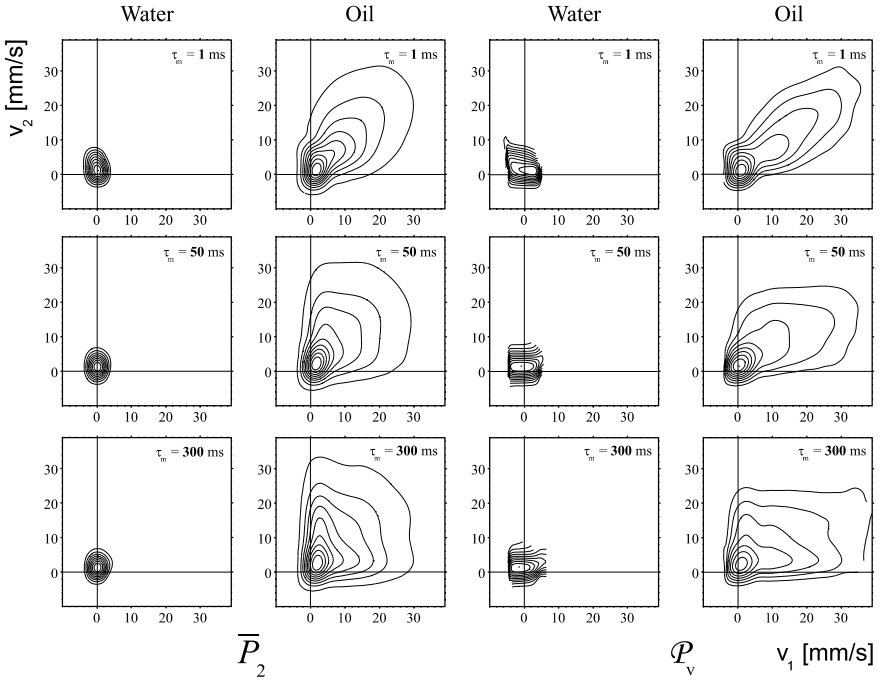

Fig. 8. Joint two-time probability densities $\overline{P_2}(Z_1, \Delta; Z_2, \Delta; \tau_m)$ (two left columns) and conditional probabilities $\mathscr{P}_V(Z_1, \Delta | Z_2, \Delta; \tau_m)$ (two right columns) for the water and oil components; conditions as in Fig. 4; $\Delta = 16$ ms.

system with a wide spread of flow velocities [28]. For the longest time, $\tau_m \approx 7\tau_c$ so that the correlation should have died away. From the observation in Fig. 8 it is concluded that this describes the behaviour of the fast particles (outermost contour lines) reasonably well. The persistent peak near zero velocity confirms the notion of a subset of particles which effectively do not change their velocity at all. This peak has also been found for single-phase flow at comparable Péclet numbers and times, albeit much less pronounced. It confirms the longer residence time of molecules in quasi-static pools in the presence of a residual phase.

If oil is replaced by water as the flowing fluid, a similar observation is made for the residual phase, leaving no trace of correlated motion (see Fig. 9, second and fourth columns). If the picture drawn above were correct, which assumes a circulating motion within dispersed fluid elements with amplitudes up to 2 mm/s, a finite slope in the plot of the conditional probability should be found at least for a certain range of mixing times. Instead, almost perfectly horizontal lines are found, much as in Fig. 8. Therefore, the internal motion within the stagnant phase must be of a more complicated nature, or appearing on short length and time scales so that they are already averaged out even for the shortest mixing time. Clearly, a more thorough investigation of two-phase flow properties is needed which pays attention particularly to the behaviour of the static phase, providing information also about the different morphology of fluids with wetting and non-wetting characteristics.

The dispersion process of the moving water phase shown in Fig. 9 can be more readily understood. The same evolution from a strong positive correlation for vanishing mixing times approaching a loss of correlation for $\tau_m = 300$ ms is found as in the case of flowing oil discussed above (see Fig. 8). Assuming the higher average velocity of water, the correlation time reduces to about 35 ms, but the difference is small enough to allow a direct comparison of the behaviour of the two flowing phases at identical times. One finds that at the central row ($\tau_m = 50$ ms), the loss of correlation in water flow is more pronounced as for the oil flow case. At $\tau_m = 300$ ms, the two plots become similar but the amplitude of the stagnant peak is higher for the flowing water phase, an effect which is mainly caused by the more pronounced water zero-velocity peak during the encoding time.

For the same conditions as described under Fig. 6, single-phase flow results of water are presented for comparison in Fig. 10. The initial correlation at vanishing mixing times is very strong, as can be seen from the preferential alignment along the main diagonal in the top row of plots. Comparing these data with the results obtained in the presence of the stagnant second (oil) phase (first row in Fig. 9), one finds that the latter shows a much more pronounced peak around zero velocity. The positive correlation between velocities is brought about by a much smaller fraction of fluid elements in the latter cases. The same observation remains true for intermediate mixing times (second row in Figs. 9 and 10). The correlation appears somewhat

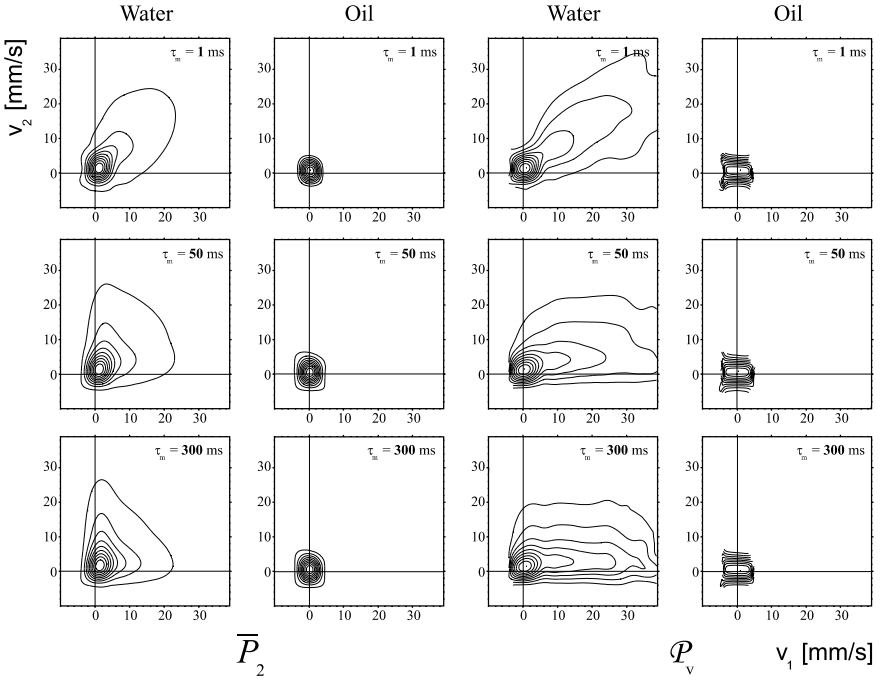

Fig. 9. Joint two-time probability densities $\overline{P_2}(Z_1, \Delta; Z_2, \Delta; \tau_m)$ (two left columns) and conditional probabilities $\mathscr{P}_V(Z_1, \Delta | Z_2, \Delta; \tau_m)$ (two right columns) for the water and oil components; conditions as in Fig. 5; $\Delta = 16$ ms.

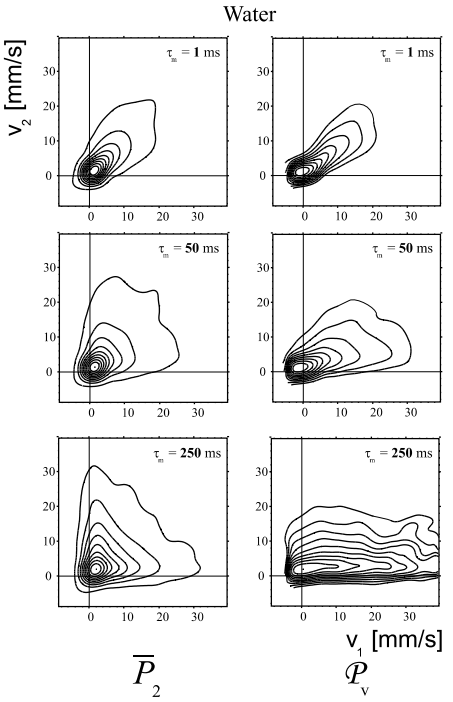

Fig. 10. Joint two-time probability densities $\overline{P_2}(Z_1, \Delta; Z_2, \Delta; \tau_m)$ (first column) and conditional probabilities $\mathscr{P}_V(Z_1, \Delta | Z_2, \Delta; \tau_m)$ (second column) for single-phase flow of water; conditions as in Fig. 6; $\Delta = 16$ ms.

weaker for the two-phase sample. This can be explained by the fact that the smaller fraction of fluid elements essentially participating in the flow processes possesses larger velocities on average, if the total volume flow rate is kept constant. They therefore travel larger distances during τ_m and are more likely to change their velocity due to dispersive effects. The VEXSY results demonstrate that the presence of a second, stagnant phase influences dispersion of the flowing phase in the sense that one fraction of molecules experiences a rapid sampling of the velocity field while the other fraction remains stagnant even for long mixing times.

If both liquids are flowing simultaneously, positive correlations are found for both of them (see Fig. 11). However, data analysis is made somewhat more difficult as compared to the cases of one non-moving component. This is due to the dominance of the low-velocity peak which is particularly persistent for the oil phase where it shows up already in the one-dimensional propagators (see Fig. 7). In the two-dimensional plots of $\overline{P_2}(Z_1, \Delta; Z_2, \Delta; \tau_m)$, this peak is much more pronounced. In order to highlight the small fraction of fast-flowing liquid, the outer contour lines are drawn in ten steps of 1% each (left two columns) and 4% each (right two columns), supplemented by lines in 10% steps up to the peak amplitude. Before, we have drawn lines in steps of 10% in Figs. 8 and 9. This corresponds to a relatively small fraction of the fluid moving with velocities considerably larger than the average value, $\overline{v^*}$. The largest velocities are not represented well anymore due to the small signal/noise ratio.

For vanishing mixing times (top row), an alignment along the main diagonal is found but it is only due to a small fraction of fluid molecules. While there is hardly any change for both phases of the stagnant fluid fraction

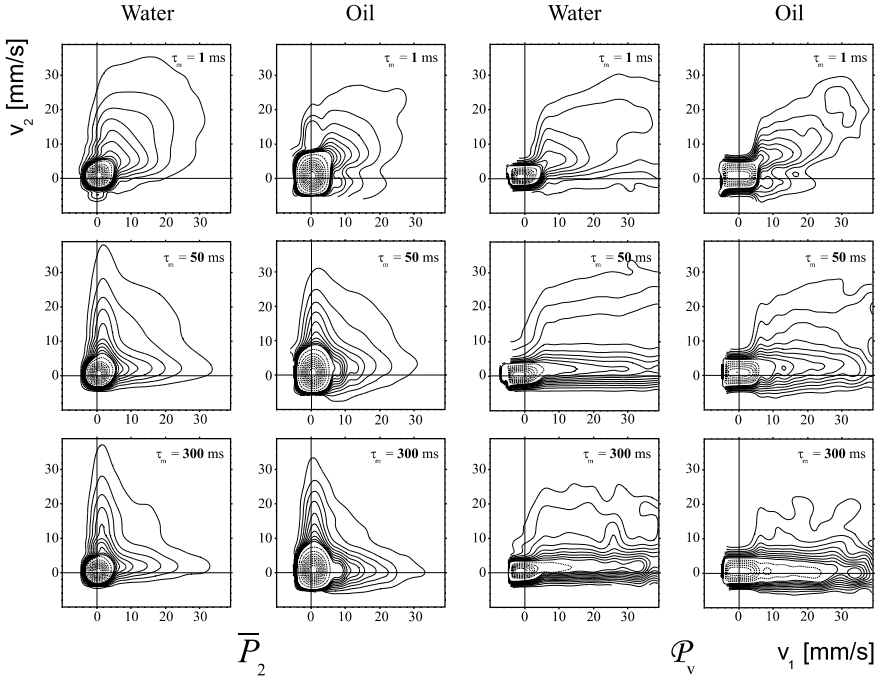

Fig. 11. Joint two-time probability densities $\overline{P_2}(Z_1, \Delta; Z_2, \Delta; \tau_m)$ (two left columns) and conditional probabilities $\mathscr{P}_V(Z_1, \Delta | Z_2, \Delta; \tau_m)$ (two right columns) for the water and oil components; conditions as in Fig. 7; $\Delta = 16$ ms.

with increasing mixing time, the loss of correlation of the moving fractions becomes much more pronounced than in any of the previously discussed cases. Already for $\tau_m = 50$ ms, the correlation has practically vanished and mostly horizontal lines are observed in the plots of the conditional probability (third and fourth column in Fig. 11). This information is not available from the one-dimensional propagators as a function of Δ, where only a relatively weak change of the high-velocity portion is seen for Δ being varied between 32 and 300 ms. Although the fraction of stagnant fluid is relatively large, in particular for the oil phase, this does not sufficiently explain the fast decrease of correlation. One possibility is the presence of non-stationary boundaries between the water and the oil phase, which inevitably lead to velocity changes of individual fluid elements. This process is superposed onto the mechanical and non-mechanical contributions to dispersion, so that the effective correlation times describing the velocity change is much reduced compared to the influence of the geometrical restrictions alone.

What becomes obvious is the clear distinction that can be made between stagnant and moving fluid. While partly visible in one-dimensional measurements, this distinction is much facilitated by the use of two-dimensional techniques. This distinction has been observed for single-phase flow where it is most prominent at very high Péclet numbers [28]. The present study shows that this distinction becomes clearer in the presence of one non-flowing phase, and even more so for two flowing phases. While for the present case, the behaviour of both fluids appears to be similar if they are flowing simultaneously, this might not be the case for a different combination of liquids and/or geometry of the pore space. On the other hand, the correlation properties are found to differ from each other if one of the phases remains stagnant. By applying chemically resolved VEXSY experiments it is possible to distinguish the different types of behaviour and to discuss the dispersion properties of both phases separately. Further studies will focus on combining the averaged description obtained from propagator and VEXSY experiments with spatial information. By varying the ratio of encoding time Δ and mixing time τ_m relative to τ_c, a wider range of dynamic processes can be monitored. This can partly be achieved by varying flow rate and bead size, but might necessitate the use of stronger PFGs in order to allow shorter encoding periods. With such an improved temporal resolution, the methods will be employed to scrutinize the possible existence of circulating motions within dispersed droplets of the isolated phase.

5. Conclusions

We have demonstrated the feasibility of performing a Velocity Exchange Spectroscopy (VEXSY) experiment with chemical resolution, thus allowing us to monitor the evolution not only of the velocity distribution function, but also of the correlation between velocities measured at different times as a function of mixing time simultaneously for both components of flow in a model porous system saturated by two fluid phases. The components (water and silicone oil with a separation of 4.8 ppm) could be clearly resolved and analyzed separately even for low residual concentrations and for the use of a packing of small (400 μm diameter) glass beads in a reasonably high magnetic field, leading to considerable susceptibility broadening. The application represents an important step towards the measurement and understanding of multiphase flow of immiscible liquids in structured media and porous solids, which is of considerable relevance in processes of reaction engineering and oil well logging. Adding the dimension of chemical resolution to a class of multiply-encoding PFG sequences to determine displacements and higher moments of motion is also a necessary requisite for gaining a much deeper insight into problems as varied as mixing processes, reaction kinetics and metabolism transport in biological samples.

Acknowledgments

The experimental part of this work has been taken out during fruitful stays of AAK at the ITMC, RWTH Aachen. We thank P.T. Callaghan, C. Eccles, and W.M. Holmes for helpful discussions. Financial support from the Deutsche Forschungsgemeinschaft (SFB 540) and the New Zealand Foundation for Research, Science and Technology is gratefully acknowledged.

References

[1] J. Kärger, W. Heink, The propagator representation of molecular transport in microporous crystallites, J. Magn. Reson. 51 (1983) 1–7.
[2] R.A. Waggoner, E. Fukushima, Magn. Reson. Imag. 14 (1996) 1085–1090.
[3] P. Mansfield, B. Issa, Fluid transport in porous rocks—1. EPI studies and a stochastic model of flow, J. Magn. Reson. A 122 (1996) 137–148.
[4] J.J. Tessier, K.J. Packer, J.F. Thovert, P.M. Adler, NMR measurements and numerical simulations of fluid transport in porous solids, AIChE J. 43 (1997) 1653–1661.
[5] U. Tallarek, D. van Dusschoten, H. Van As, E. Bayer, G. Guiochon, Study of transport phenomena in chromatographic columns by pulsed field gradient NMR, J. Phys. Chem. B 102 (1998) 3486–3497.
[6] M.D. Mantle, A.J. Sederman, L.F. Gladden, Chem. Eng. Sci. 56 (2001) 523.
[7] S. Han, S. Stapf, B. Blümich, Two-dimensional PFG NMR for encoding correlations of position, velocity and acceleration in fluid transport, J. Magn. Reson. 146 (2000) 169–180.
[8] S. Stapf, K.J. Packer, R.G. Graham, J.F. Thovert, P.M. Adler, Spatial correlations and dispersion for fluid transport through packed glass beads, Phys. Rev. E 58 (1998) 6206–6221.

[9] S. Stapf, K.J. Packer, S. Békri, P.M. Adler, Two-dimensional NMR measurements and numerical simulations of fluid transport in porous rocks, Phys. Fluids 12 (2000) 566–580.
[10] P.T. Callaghan, B. Manz, Velocity exchange spectroscopy, J. Magn. Reson. A 106 (1994) 260–265.
[11] P.T. Callaghan, S.L. Codd, J.D. Seymour, Spatial coherence phenomena arising from translational spin motion in gradient spin echo experiments, Concepts Magn. Reson. 11 (1999) 181–202.
[12] A. Caprihan, J.D. Seymour, Correlation time and diffusion coefficient imaging: Application to a granular flow system, J. Magn. Reson. 144 (2000) 96–107.
[13] S. Han, B. Blümich, Two-dimensional representation of position, velocity and acceleration by PFG-NMR, Appl. Magn. Reson. 18 (2000) 101–114.
[14] P.P. Mitra, Multiple wave-vector extensions of the NMR pulsed-field gradient spin-echo diffusion measurement, Phys. Rev. B 51 (1995) 15074–15078.
[15] S. Stapf, R.A. Damion, K.J. Packer, Time correlations in fluid transport obtained by sequential rephasing gradient pulses, J. Magn. Reson. 137 (1999) 316–323.
[16] L. Frydman, J.S. Harwood, D.N. Garnier, G.C. Chingas, Position-displacement correlations in fluids from magnetic resonance gradient-echo shapes, J. Magn. Reson. A 101 (1994) 240–248.
[17] S. Stapf, Determination of velocity autocorrelation functions by multiple data acquisition in NMR pulsed-field gradient experiments, J. Magn. Reson. 152 (2001) 308–312.
[18] P.T. Callaghan, Principles of Nuclear Magnetic Resonance Microscopy, Clarendon Press, Oxford, 1991.
[19] A.A. Khrapitchev, P.T. Callaghan, Double PGSE NMR with stimulated echoes: phase cycles for the selection of desired encoding, J. Magn. Reson. 152 (2001) 259–268.
[20] B. Blümich, P.T. Callaghan, R.A. Damion, S. Han, A.A. Khrapitchev, K.J. Packer, S. Stapf, Two-dimensional NMR of velocity exchange: VEXSY and SERPENT, J. Magn. Reson. 151 (2001) 162–167.
[21] Y.E. Kutsovsky, L.E. Scriven, H.T. Davis, B.E. Hammer, NMR imaging of velocity profiles and velocity distributions in bead packs, Phys. Fluids 8 (1996) 863–871.
[22] L. Lebon, L. Oger, J. Leblond, J.P. Hulin, N.S. Martys, L.M. Schwartz, Pulsed gradient NMR measurements and numerical simulation of flow velocity distribution in sphere packings, Phys. Fluids 8 (1996) 293–301.
[23] L. Lebon, J. Leblond, J.P. Hulin, Experimental measurement of dispersion processes at short times using a pulsed field gradient NMR technique, Phys. Fluids 9 (1997) 481–490.
[24] S. Han, S. Stapf, B. Blümich, NMR imaging of falling water drops, Phys. Rev. Lett. 87 (2001) 144501/1-4.
[25] J.J. Tessier, K.J. Packer, The characterization of multiphase fluid transport in a porous solid by pulsed gradient stimulated-echo nuclear magnetic resonance, Phys. Fluids 10 (1998) 75–85.
[26] R.A. Damion, K.J. Packer, K.S. Sorbie, S.R. McDougall, Pore-scale network modelling of flow propagators derived from pulsed magnetic field gradient spin-echo NMR measurements in porous media, Chem. Eng. Sci. 55 (2000) 5981–5998.
[27] J.D. Seymour, P.T. Callaghan, Generalized approach to NMR analysis of flow and dispersion in porous media, AIChE J. 43 (1997) 2096–2111.
[28] A.A. Khrapitchev, S. Stapf, P.T. Callaghan, NMR visualisation of displacement correlations, Phys. Rev. E, in press.
[29] R.S. Maier, D.M. Kroll, R.S. Bernard, S.E. Howington, J.F. Peters, H.T. Davis, Pore-scale simulation of dispersion, Phys. Fluids 12 (2000) 2065–2079.